



How does a valine residue that modulates heme-NO binding kinetics in inducible NO synthase regulate enzyme catalysis?

Zhi-Qiang Wang^{a,*}, Chin-Chuan Wei^b, Dennis J. Stuehr^{c,*}

^a Department of Chemistry, Kent State University Tuscarawas, New Philadelphia, OH 44663, United States

^b Department of Chemistry, Southern Illinois University Edwardsville, Edwardsville, IL 62026, United States

^c Department of Pathobiology, Lerner Research Institute, Cleveland Clinic Foundation, Cleveland, OH 44195, United States

ARTICLE INFO

Article history:

Received 30 June 2009

Received in revised form 6 November 2009

Accepted 11 November 2009

Available online 18 November 2009

Keywords:

Nitric oxide

NO synthesis

Mechanism

Mutation

Catalysis

ABSTRACT

Nitric oxide (NO) release from nitric oxide synthases (NOSs) depends on the dissociation of a ferric heme-NO product complex (Fe^{III}NO) that forms immediately after NO is made in the heme pocket. The NOS-like enzyme of *Bacillus subtilis* (bsNOS) has 10–20 fold slower Fe^{III}NO dissociation rate (k_d) and NO association rate (k_{on}) compared to mammalian NOS counterparts. We previously showed that an Ile for Val substitution at the opening of the heme pocket in bsNOS contributes to these differences. The complementary mutation in mouse inducible NOS oxygenase domain (Val346Ile) decreased the NO k_{on} and k_d by 8 and 3-fold, respectively, compared to wild-type iNOSoxy, and also slowed the reductive processing of the heme-O₂ catalytic intermediate. To investigate how these changes affect steady-state catalytic behaviors, we generated and characterized the V346I mutant of full-length inducible NOS (iNOS). The mutant exhibited a 4–5 fold lower NO synthesis activity, an apparent uncoupled NADPH consumption, and formation of a heme-NO complex during catalysis that was no longer sensitive to solution NO scavenging. We found that these altered catalytic behaviors were not due to changes in the heme reduction rate or in the stability of the enzyme heme-O₂ intermediate, but instead were due to the slower NO k_{on} and k_d and a slower oxidation rate of the enzyme ferrous heme-NO complex. Computer simulations that utilized the measured kinetic values confirmed this interpretation, and revealed that the V346I iNOS has an enhanced NADPH-dependent NO dioxygenase activity that converts almost 1 NO to nitrate for every NO that the enzyme releases into solution. Together, our results highlight the importance of heme pocket geometry in tuning the NO release versus NO dioxygenase activities of iNOS.

© 2009 Elsevier Inc. All rights reserved.

1. Introduction

Nitric oxide synthases (NOSs) are flavo-heme enzymes that catalyze a stepwise oxidation of L-arginine (Arg) to form nitric oxide NO and L-citrulline [1–3]. The overall biosynthetic reaction consumes 1.5 NADPH and 2 O₂ and involves two steps: the first being Arg hydroxylation to form N-hydroxy-L-Arg (NOHA), and the second being NOHA oxidation to form citrulline and NO (Scheme 1). NOSs are homodimeric enzymes [4,5], with each monomer being comprised of an N-terminal oxygenase domain that binds Fe-protoporphyrin IX (heme), the substrate Arg, and the cofactor 6R-tetrahydrobiopterin (H₄B) [6,7], and a C-terminal flavoprotein domain that binds FAD, FMN, and NADPH [8–10], with the two domains being linked by a central calmodulin (CaM) binding motif [5,11,12]. The heme is ligated to a cysteine thiolate and acts in conjunction with H₄B to catalyze a reductive activation of molecular

oxygen in both steps of NO synthesis [13–15]. During catalysis, the ferric heme is reduced to ferrous by the flavoprotein domain and then binds O₂ to form a heme-superoxy species, this intermediate is then further reduced by H₄B, which enables formation of reactive heme-peroxy or Iron (IV)-oxo porphyrin radical cation (often referred as Compound 1) species that react with substrate Arg or NOHA.

In general, the slow step in NO biosynthesis is limited by the rate of ferric heme reduction (k_r) as catalyzed by the NOS flavoprotein domain. However, NOS activity is also influenced in a fundamental way by a heme-NO binding event that is an intrinsic feature of their catalysis [16–20]. Each newly-generated NO molecule has a high probability of binding to the NOS heme multiple times before it escapes from the heme pocket [21,22], and even NO released from the enzyme can rebound to the NOS heme if sufficient external concentrations are achieved (low μ M NO) [19,22]. Accordingly, NOS heme-NO complexes can build up both in steady-state reactions and as a transient species during NOHA oxidation reactions catalyzed by NOS oxygenase domains (NOSoxy) under single turnover conditions [16–19].

* Corresponding authors. Tel.: +1 216 445 6950; fax: +1 216 636 0104 (D.J. Stuehr), tel.: +1 330 308 7564; fax: +1 330 339 5022 (Z.-Q. Wang).

E-mail addresses: zwang3@kent.edu (Z.-Q. Wang), stuehrd@ccf.org (D.J. Stuehr).

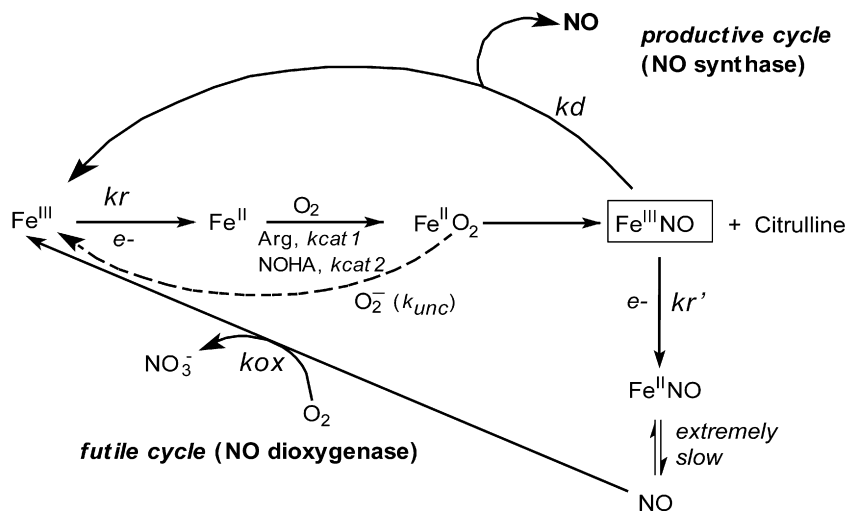
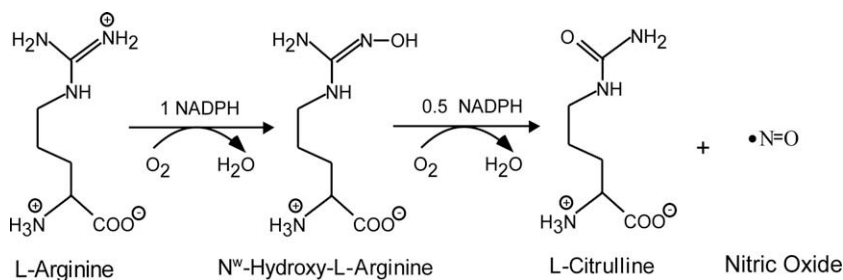


Fig. 1. Global kinetic model for NO synthesis by NOS. During steady-state catalysis, the enzyme molecules engage in a productive cycle that releases free NO and in a futile cycle that releases a higher oxide of nitrogen (nitrate). Reduction of ferric enzyme to ferrous (k_r) enables the heme to bind O_2 and initiates catalytic reactions. k_{cat1} and k_{cat2} are the conversion rates of the $Fe^{II}O_2$ species to products in the Arg hydroxylation and NOHA oxidation reactions, respectively. After NO is made, an immediate product of catalysis is the ferric heme-NO complex ($Fe^{III}NO$), which can either release NO (k_d) or become reduced (k_r') to generate a ferrous heme-NO complex ($Fe^{II}NO$). The ferrous heme-NO complex dissociates extremely slowly and instead regenerates the active ferric enzyme by reacting with O_2 (k_{ox}). The $Fe^{II}O_2$ intermediate can also undergo an uncoupled reaction that generates ferric enzyme and superoxide (k_{unc}).

Intrinsic heme-NO binding makes NOS catalysis a blended function of the rates of heme reduction (k_r or k_r'), reduction of the heme-superoxy complex by H₄B (k_{cat}), ferric heme-NO dissociation (k_d), and ferrous heme-NO oxidation by O_2 (k_{ox}), according to the model shown in Fig. 1 [23,24]. The model stipulates that the k_r , k_{cat} , k_d , and k_{ox} parameters must be balanced in order for NOS enzymes to release NO and minimize destruction of NO via a NO dioxygenase reaction that generates nitrate, as described by the futile cycle in Fig. 1. Interestingly, the set points for k_r , k_{cat} , k_d , k_{ox} vary among NOS enzymes [23,25] and give each NOS a unique catalytic profile probably to aid their specific functions in biology [26–28].

Some protein features that help determine set points for the k_r , k_{cat} , k_d , and k_{ox} kinetic parameters in NOS enzymes have been identified [18,20,29,30]. Regarding k_d , the variation among the mammalian NOS enzymes is relatively small (2 or 3-fold), but the *Bacillus subtilis* NOS exhibits a 10–20 fold slower k_d compared to the mammalian NOS enzymes [31]. We showed previously that this difference is partly due to a Val to Ile substitution that is conserved among bacterial NOS enzymes and restricts NO from entering or exiting the distal heme pocket [31]. When we incorporated the complementary V346I substitution into the inducible NOS oxygenase domain (iNOSoxy), it decreased the NO k_d about 3-fold, diminished the rates of solution NO or O_2 binding to the iNOSoxy heme, and slowed down the reduction of the enzyme's heme-superoxy intermediate (k_{cat}) in single turnover experiments (Table 3), and also increased the extent of geminate or near-geminate heme-NO binding in flash photolysis studies [22]. Because all these

studies used the V346I iNOSoxy protein, we were unable to measure how the kinetic changes might influence the catalytic behavior of iNOS. We therefore generated and characterized V346I iNOS regarding its steady-state catalytic activities, electron flux, k_r and k_{ox} parameters, heme-NO complex formation, and stability of its heme-superoxy intermediate. We then utilized the measured values in computer simulations of the model in Fig. 1 [23,24] to understand the catalytic behavior of V346I iNOS. Our results show: (i) the V346I mutant has a 4-fold lower NO synthesis activity compared to wild-type iNOS and (ii) the lower activity can be primarily explained by the changes in the k_d and k_{ox} kinetic parameters, which cause a greater proportion of V346I iNOS to cycle through the futile pathway and function as an NO dioxygenase. This in turn causes a greater proportion of the biosynthesized NO to be oxidized to nitrate instead of being released from the enzyme as NO.

2. Materials and methods

2.1. Materials

All reagents and materials were obtained from Sigma, Aldrich, Alexis, or sources described previously [17,30,32].

2.2. Mutagenesis

Site-directed mutagenesis of mouse $\Delta 65$ iNOS full length DNA in the pCWori expression plasmid (coding for amino acids 65–1269

plus a His₆ tag at the N terminus) were performed using the Quik-Change site-directed mutagenesis Kit from Stratagene. Forward and reverse primers used are listed in our previous paper [31]. The mutations were confirmed at the molecular biology core facility of the Cleveland Clinic by sequencing about 500 consecutive base pairs including the mutation sites. No other mutations were observed. DNA isolation, restriction enzyme digestion, and transformation were carried out using standard protocols [33].

2.3. Protein expression and purification

Wild-type iNOS enzymes and mutants were overexpressed in *Escherichia coli* BL21 and purified using Ni²⁺-nitrilotriacetate affinity chromatography as reported previously [16,34]. NOS concentrations were determined from the 444 nm absorbance of the ferrous–CO complex, using an extinction coefficient 76 mM⁻¹ cm⁻¹ [35]. Buffer used for all experiments in this manuscript was 40 mM Epps (pH 7.6) containing 250 mM NaCl and 10% glycerol.

2.4. NO synthesis and NADPH oxidation rates

Steady-state rates of NO synthesis were determined by the spectrophotometric oxyhemoglobin assay using a difference extinction coefficient of 38 mM⁻¹ cm⁻¹ for the oxyhemoglobin to methemoglobin transition at 401 nm [18,36]. Sample solutions contained 0.1 μM NOS enzyme, 20 μM H₄B, 5 mM Arg, 0.3 mM DTT, 0.1 mg/ml BSA, 10 U/ml SOD, 346 U/ml catalase, 10 μM oxyhemoglobin, 4 μM FMN and FAD. Reactions were initiated by adding NADPH (100 μM final concentration), and the absorbance change at 401 nm was recorded at room temperature. For the NADPH oxidation rate measurements we used an extinction coefficient of 6.22 mM⁻¹ cm⁻¹ at 340 nm. In some cases 0.3 mM NOHA or 1 mM L-NAME were added in the reaction solution in place of Arg.

2.5. Rates of heme reduction

The kinetics of ferric heme reduction was determined as described previously [20,36]. Reactions were carried out in a Hi-Tech SF-61 stopped-flow apparatus equipped for anaerobic work and coupled to a Hi-Tech MG-6000 diode array detector. Reactions were initiated by rapid mixing an anaerobic ferric enzyme solutions containing ~2 μM NOS, 100 μM H₄B, 4 mM Arg, 1.2 mM DTT with an anaerobic CO-saturated buffer solution containing 100 μM NADPH at 10 °C. Heme reduction was followed by the absorbance increase at 444 nm due to formation of the ferrous–CO complex.

2.6. Single catalytic turnover reactions

An anaerobic solution that contained the 4–5 μM dithionite-reduced enzyme, 0.6 mM DTT, 0.5 mM Arg or 0.4 mM NOHA and 0.2 mM H₄B or H₂B was transferred into the stopped-flow instrument and rapidly mixed with air-saturated Epps buffer at 10 °C, as reported previously [37,42]. Ninety-six spectral scans were obtained after each mixing. Sequential spectral data were fit to different reaction models using the Specfit global analysis program (provided by Hi-Tech Ltd.), which could calculate the number of different enzyme species, their spectra, and their concentrations versus time during the single turnover reactions. In the presence of NOHA and H₄B, the spectral data best fit to an A (Fe^{III}) → B (Fe^{II}O₂) → C (Fe^{III}NO) → D (Fe^{III}) model. In all other cases, the spectral data best fit to an A (Fe^{III}) → B (Fe^{II}O₂) → C (Fe^{III}) model. Data from 8 to 10 sequential reactions were averaged to obtain the rates of the various heme transitions (Fe^{II}O₂) [30,31].

2.7. Ferrous heme-NO complex oxidation

Wild-type iNOSox and V346I iNOSox protein solutions (~4 μM) containing 5 mM Arg and 200 μM H₄B were made anaerobic and reduced with dithionite in an anaerobic optical cell [13,31]. The ferrous proteins were then titrated by adding small amounts of anaerobic NO-saturated buffer to form the ferrous NO complex, which were transferred to the stopped-flow instrument using a gastight syringe and rapid-mixed with air-saturated or oxygen-saturated buffer at 10 °C [23,38]. Sequential spectral scans were collected and fit to an A→B reaction model using the Specfit global analysis program. Eight to ten scans were analyzed and then averaged for each experimental condition.

2.8. Effect of a superoxide-generating system on the heme-NO complex formation

The iNOS wild type or mutant proteins (2 μM) were incubated with 40 μM H₄B, 2 mM Arg and 1.2 mM hypoxanthine at room temperature for 5 min. Thirty seconds after xanthine oxidase (0.1 U/ml) was added to the reaction solution, 120 μM NADPH was added to initiate NO synthesis [19]. Heme-NO complex formation was monitored at 437 nm. Control experiments were done by replacing xanthine oxidase with equal amount of buffer.

2.9. Nitrite and nitrate production in NADPH-driven reactions

Solutions (90 μL) containing 3 nM wild-type iNOS or 8 nM V346I, 20 μM H₄B, 3 mM Arg, 0.3 mM DTT, 0.1 mg/ml BSA, 10 U/ml SOD, 346 U/ml catalase, 4 μM FMN and FAD were added into a 96-well microplate and incubated on ice for 30 min. The reaction was initiated by adding 10 μl 10 mM NADPH. After reacting for 30 min in 37 °C incubator, excess NADPH was consumed by addition of 10 U/ml lactate dehydrogenase (LDH) and 10 mM sodium pyruvate. Absorbance difference at 550 and 650 nm were measured using a microplate reader after adding Griess reagent (0.1% NED solution and 1% sulfanilamide in 4.25% H₃PO₄) to each well. Nitrite production was quantitated based on the standard curve of nitrite solutions standard curve [39,40].

Total amount of nitrite and nitrate were determined using a similar method except adding nitrate reductase (0.1 U/ml) and incubating the samples for extra 2 h at 37 °C before the addition of LDH and sodium pyruvate [41]. Nitrate production was calculated by subtracting the nitrite amount from the total amount of nitrite plus nitrate.

2.10. Simulations of enzyme distribution during steady-state NO synthesis

Computer simulations were based on the global kinetic model described in Fig. 1 and were run using Mathcad 7.0 software. The detailed equations are described in our previous papers [23,24,27]. Simulations used constant values for O₂ concentration (280 μM) and NADPH concentration (40 μM) to avoid secondary effects due to their exhausting. Values of ferric heme reduction (k_r), ferrous heme-NO oxidation (k_{ox}), heme-NO dissociation (k_d), NO association to the ferric enzyme (k_{on}), catalytic rate constant (k_{cat1} , k_{cat2}), Fe^{II}O₂ intermediate decay rate in uncoupling reaction (k_{unc}) used for simulation are listed in Tables 2 and 3. O₂ binding constant and NO release rate from Fe^{II}NO are $3.5 \times 10^5 \text{ M}^{-1} \text{ s}^{-1}$ and $1.35 \times 10^{-4} \text{ s}^{-1}$, respectively. In some cases, 10 μM NO were set for the simulations to take solution NO binding to the ferric enzyme into account.

3. Results and discussion

3.1. NO synthesis and NADPH oxidation

We measured steady-state rates of NO synthesis and NADPH oxidation at 25 °C with Arg or the intermediate NOHA serving as the substrate (Table 1). The V346I iNOS had a 4–5 fold lower NO synthesis activity with either substrate as compared to the wild-type iNOS. This was not related to poor substrate binding because the mutant Arg binding affinity is similar to wild-type iNOS [31]. The corresponding NADPH oxidation rates were also lower in V346I iNOS, suggesting it has a slower electron flux through the heme. The lower catalytic activities are similar to results published for an analogous mutant of neuronal NOS (V567L) [43].

NO synthesis from Arg and NOHA has a theoretical minimum stoichiometry of 1.5 and 0.5 NADPH oxidized per NO formed, respectively [11,44]. We observed stoichiometries similar to these minimal values for wild-type iNOS (Table 1), whereas we observed values of 3.9 and 1.5 NADPH oxidized per NO formed from Arg and NOHA, respectively, for V346I iNOS. Control experiments that substituted the heme reduction inhibitor L-NAME [45] for Arg indicated that the mutant does not catalyze greater NADPH oxidation under this circumstance (Table 1). This implies the excess NADPH consumption in V346I iNOS is due to some of its heme reduction (or electron flux through its heme) being uncoupled either from NO biosynthesis or from NO release.

3.2. Kinetics of heme reduction (k_r)

To better understand the catalytic behaviors of V346I iNOS, we measured the kinetics of heme reduction (k_r) in a stopped-flow spectrophotometer by mixing ferric V346I or wild-type iNOS that contained bound Arg and H₄B with excess NADPH in the presence of CO-saturated buffer under anaerobic conditions [46,47]. Formation of the heme Fe^{II}CO complex was followed at 444 nm. Fig. 2 contains representative spectra and absorbance kinetic traces at 444 nm. A comparison of the beginning and ending spectral traces indicate that a similar extent of heme reduction occurred for both V346I and wild-type iNOS. The initial absorbance decrease in each kinetic trace is due to flavin reduction that always takes place before electrons can transfer to the ferric heme [17,18]. The rate of the absorbance increases fit well to a monophasic equation and gave k_r values of $0.69 \pm 0.02 \text{ s}^{-1}$ and $0.64 \pm 0.02 \text{ s}^{-1}$ for wild-type and the V346I iNOS, respectively (Table 2). This means the Va-

Table 3

Calculated k_{cat} and k_{unc} rates ($\text{Fe}^{\text{II}}\text{O}_2$ decay, s^{-1}) during single turnover reactions at 10 °C. Ferrous WT and V346I iNOSoxy proteins containing substrates Arg/NOHA and the indicated pteridine were rapid-mixed at 10 °C with air-saturated buffer to start the reactions. Subsequent heme transitions were followed by stopped-flow rapid-scanning spectroscopy. Rates were calculated by Specfit global analysis of diode array spectral data. Values are the means \pm SD of three determinations. WT, wild type.

Substrate + cofactor (rate)	Enzymes	
	WT	V346I
H ₄ B + Arg ($\text{Fe}^{\text{II}}\text{O}_2 \rightarrow \text{Fe}^{\text{III}}$, $k_{\text{cat}1}$)	12.5 ± 0.2	3.68 ± 0.17
H ₄ B + NOHA ($\text{Fe}^{\text{II}}\text{O}_2 \rightarrow \text{Fe}^{\text{III}}\text{NO}$, $k_{\text{cat}2}$)	36.7 ± 1.1	4.51 ± 0.19
H ₂ B + NOHA ($\text{Fe}^{\text{II}}\text{O}_2 \rightarrow \text{Fe}^{\text{III}} + \text{O}_2^-$, k_{unc})	11.0 ± 0.1	2.34 ± 0.20
H ₂ B + Arg ($\text{Fe}^{\text{II}}\text{O}_2 \rightarrow \text{Fe}^{\text{III}} + \text{O}_2^-$, k_{unc})	0.30 ± 0.08	0.023 ± 0.001

I346Ile mutation does not alter the rate or extent of heme reduction in iNOS.

3.3. Stability of the heme-superoxy intermediate

It is conceivable that the increased NADPH consumption and lower NO synthesis activity of V346I iNOS is due to increased decay of its heme-superoxy intermediate in an uncoupled reaction that generates ferric enzyme and superoxide (k_{unc} in Fig. 1). Specifically, the relatively slow reduction of the heme-superoxy intermediate in V346I iNOS (as indicated by the slow k_{cat}) may make it more susceptible to this uncoupled decay. We examined the stability of the heme-superoxy intermediate by forming it in V346I iNOSoxy in a stopped-flow spectrophotometer and then monitoring its transition back to ferric enzyme by an established method [30] (data not shown). The enzyme contained H₂B in place of H₄B so as to prevent the reductive processing of the heme-superoxy intermediate that would otherwise occur if H₄B is present in the enzyme [30]. The rate measurements (Table 3) indicate that the heme-superoxy intermediate of V346I iNOSoxy is actually 8–13 times more stable than that of wild-type iNOSoxy. Thus, the lower NO synthesis activity and increased NADPH consumption of V346I iNOS is not due to an uncoupled decay of its heme-superoxy intermediate.

3.4. Oxidation rate of the ferrous heme-NO complex (k_{ox})

We next determined k_{ox} for the wild-type and V346I iNOSoxy proteins by mixing their ferrous heme-NO complexes with an air-saturated or oxygen-saturated buffer in the stopped-flow spec-

Table 1
NO synthesis and NADPH oxidation activities in the presence of different substrates and an inhibitor. Rates were measured at 25 °C as described under Section 2. The turnover number is expressed as the moles of product formed per mole of heme per minute. Data are the mean and standard deviation of three determinations. WT, wild type.

Enzyme	H ₄ B + Arg		H ₄ B + NOHA		H ₄ B + L-NAME	
	NO synthesis (min ⁻¹)	NADPH oxidation (min ⁻¹)	NO synthesis (min ⁻¹)	NADPH oxidation (min ⁻¹)	NO synthesis (min ⁻¹)	NADPH oxidation (min ⁻¹)
WT iNOS	70 ± 5	119 ± 5	131 ± 7	75 ± 4	0	13 ± 1
V346I	15 ± 1	59 ± 2	24 ± 1	36 ± 2	0	6 ± 1

Table 2
Kinetic parameters of iNOS and the V346I mutant. Rates were measured at 10 °C as described under Section 2. Data are the mean and standard deviation of three determinations. WT, wild type.

NOS	Heme reduction k_r (s^{-1}) ^a	Fe ^{II} NO oxidation k_{ox} (s^{-1}) ^a	NO dissociation k_d (s^{-1}) ^b	NO association k_{on} ($\mu\text{M}^{-1} \text{ s}^{-1}$) ^b	NO Keq ^c (μM)
WT	0.64 ± 0.02	3.11 ± 0.15	2.3 ± 0.1	0.27 ± 0.03	8 ± 0.3
V346I	0.69 ± 0.02	1.81 ± 0.01	0.77 ± 0.03	0.033 ± 0.003	23 ± 1

^a Measured in this paper.

^b Data are adapted from Ref. [31].

^c Keq = k_d/k_{on} .

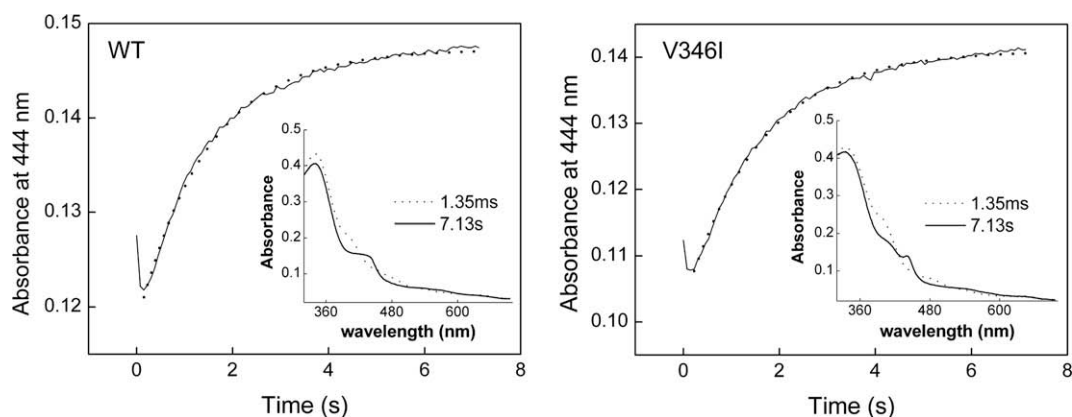


Fig. 2. Kinetics of ferric heme reduction. Anaerobic ferric enzyme solutions containing 100 μM H_4B , 4 mM Arg, 1.2 mM DTT, and $\sim 2 \mu\text{M}$ NOS were rapid-mixed with an anaerobic CO-saturated buffer solution containing 100 μM NADPH at 10 $^\circ\text{C}$. Heme reduction was followed by formation of the ferrous-CO complex at 444 nm. Dotted lines are the fitted curves. Inset plots show the spectra of enzymes recorded at two different time points during the reaction, as indicated in the figure.

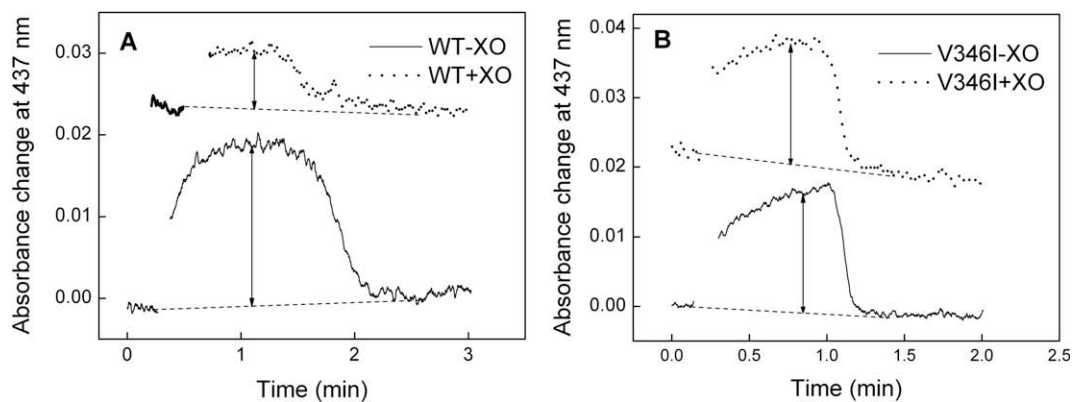


Fig. 3. Heme-NO complex formation during catalysis and the effect of solution NO buildup. Reactions were initiated by adding 120 μM NADPH to 2 μM enzyme solution containing 40 μM H_4B , 2 mM Arg, 1.2 mM hypoxanthine and in some cases 0.1 U/ml Xanthine oxidase (XO). Heme-NO complex formation was monitored at 437 nm. Solid lines showed heme-NO complex formation in the absence of Xanthine oxidase and dotted lines are with Xanthine oxidase. The data represent at least three experiments each.

trophotometer, and following their subsequent conversion to ferric enzyme [20,23]. The starting $\text{Fe}^{\text{II}}\text{NO}$ complex and ending ferric enzyme was observed for both proteins, and their conversion fit well to a monophasic transition (data not shown). The calculated k_{ox} values under an air-saturated buffer system are listed in Table 2. The k_{ox} of the V346I mutant was about half that of wild-type iNOS-oxo at both O_2 concentrations (data for O_2 -saturated buffer not shown). This difference is consistent with the Val346Ile mutation restricting O_2 access into the heme pocket [31] in order to react with the ferrous heme-NO complex. The slower k_{ox} of V346I iNOS should cause it to cycle more slowly through the futile cycle (Fig. 1). However, the k_{ox} in the mutant is still sufficiently fast relative to the k_{r} such that significant buildup of the enzyme heme $\text{Fe}^{\text{II}}\text{NO}$ complex is not able to occur during steady-state NO synthesis. Thus, the slower k_{ox} of V346I iNOS, on its own, may not greatly alter the distribution of the enzyme molecules during steady-state NO synthesis.

3.5. Heme-NO complex formation during catalysis and the effect of solution NO buildup

During steady-state NO synthesis by iNOS, the ferric form is the predominant species and will bind solution NO if the NO concentration reaches a sufficient level during the reaction [19]. Because V346I iNOS has a slower NO k_{d} and k_{on} , and also a slower k_{ox} , compared to wild-type iNOS (Table 2), we compared the extents of

their heme-NO complex buildup during NO synthesis under conditions where NO was or was not allowed to accumulate in the reaction solution. The solution NO was scavenged by inclusion of a xanthine oxidase superoxide-generating system, as utilized previously with wild-type iNOS [19]. Enzyme heme-NO complex formation was monitored by the absorbance gain at 437 nm, which approximates the Soret maximum for the NOS ferric and ferrous heme-NO complexes. As shown in Fig. 3A, heme-NO complex accumulated in wild-type iNOS during NO synthesis, but accumulated to a significantly lesser extent (30% of control) when the solution NO was scavenged during the reaction, consistent with our previous findings [19]. In comparison, a slightly lesser degree of heme-NO complex buildup was observed in the V346I iNOS reaction, and this level did not measurably change when the solution NO was scavenged (Fig. 3B). The difference between wild-type and mutant is consistent with the observed changes in the NO k_{d} and k_{on} , and k_{ox} parameters for V346I iNOS. Specifically, the altered kinetic values disfavor formation of a heme-NO complex via solution NO binding (the K_{eq} for NO is three-times higher in V346I iNOS, see Table 2), which otherwise is the predominant process in the wild-type iNOS reaction and is susceptible to solution NO scavenging. Instead, the heme-NO complex accumulates in V346I iNOS via internal heme-NO binding reactions, as enabled mainly by the slower dissociation of the ferric heme-NO product complex (k_{d}), and also by the slower oxidation rate of the ferrous heme-NO species (k_{ox}).

3.6. Nitrate and nitrite production

The slower k_d of V346I iNOS indicates that it should enter the futile cycle more often relative to wild-type iNOS (Fig. 1) and therefore have a proportionally greater NO dioxygenase activity. Because NO oxidation in solution yields nitrite, whereas the NO dioxygenase reaction of NOS yields nitrate [48], the nitrite to nitrate ratio can approximately indicate what proportion of a NOS enzyme is cycling through the productive versus futile cycles. When we compared nitrite and nitrate production by V346I and wild-type iNOS, we found a similar amount of nitrite and nitrate was formed in the wild-type enzyme reaction (Table 4). This is consistent with its k_d to k_r partition ratio somewhat favoring the productive cycle (NO dissociation and release). In contrast, nitrate was clearly the predominant product in the V346I iNOS reaction (Table 4). This is consistent with its slower k_d causing a greater proportion of the mutant enzyme to not release its NO and instead enter the futile cycle and function as an NO dioxygenase.

3.7. Simulation of steady-state catalysis and enzyme distribution

We utilized a computer simulation model based on Fig. 1 that we developed previously [23,24] to examine how all the measured changes in the kinetic parameters of V346I iNOS would alter the

Table 4

Nitrite and nitrate production in NADPH-driven reactions at 25 °C. Reactions were run for 30 min prior to quenching as described under Section 2. The values are the mean \pm SD of three measurements. WT, wild type.

NOS	NO ₂ ⁻ produced (mol/mol NOS)	NO ₃ ⁻ produced (mol/mol NOS)	NO ₂ ⁻ /NO ₃ ⁻
WT iNOS	11,300	9300	1.2:1
V346I	2400	6800	0.35:1

steady-state enzyme distribution and catalytic behaviors relative to wild-type iNOS. In addition, the simulations were run under the condition of either having no buildup of NO in the reaction solution (akin to having present oxyhemoglobin or the superoxide-generating system), or having 10 μ M NO present in the solution. The results of these simulations are summarized in Fig. 4 and Table 5.

In the simulations with no solution NO buildup, the greatest difference among the enzyme distribution patterns during NO synthesis is that the mutant has a greater buildup of both its ferric and ferrous heme-NO complexes, and proportionally less ferric enzyme present during the steady state. This difference as indicated by the simulation mimics what we observed for the mutant and wild-type iNOS reactions when their solution NO was being scavenged by an added superoxide-generating system (see Fig. 3). The simulations done with 10 μ M solution NO indicate that the enzyme distributions would change significantly. The wild-type iNOS would have much more buildup of heme-NO complexes, mostly due to an increase in its ferric heme-NO complex. In comparison, there would be a smaller increase in the total heme-NO complexes in the V346I mutant that is due to a modest increase of both its ferrous and ferric heme-NO complexes. This simulated result also mimics what we observed for the two enzymes when solution NO was allowed to accumulate in the reactions (see Fig. 3). Related simulations that calculate the enzyme distribution patterns over a wider range of solution NO concentrations are reported in Table S1. Together, the simulation results confirm that the measured changes in the k_d , k_{on} , and k_{cat} kinetic parameters of V346I iNOS can explain its altered enzyme distribution pattern during NO synthesis both in the absence or presence of solution NO.

The simulations can also predict the extent of productive versus futile cycling that occurs during steady-state NO synthesis for the wild-type and V346I iNOS enzymes. These are indicated by the calculated citrulline per NO, nitrate per citrulline, and nitrate per NO ratios that are listed in Table 5. The calculations that were

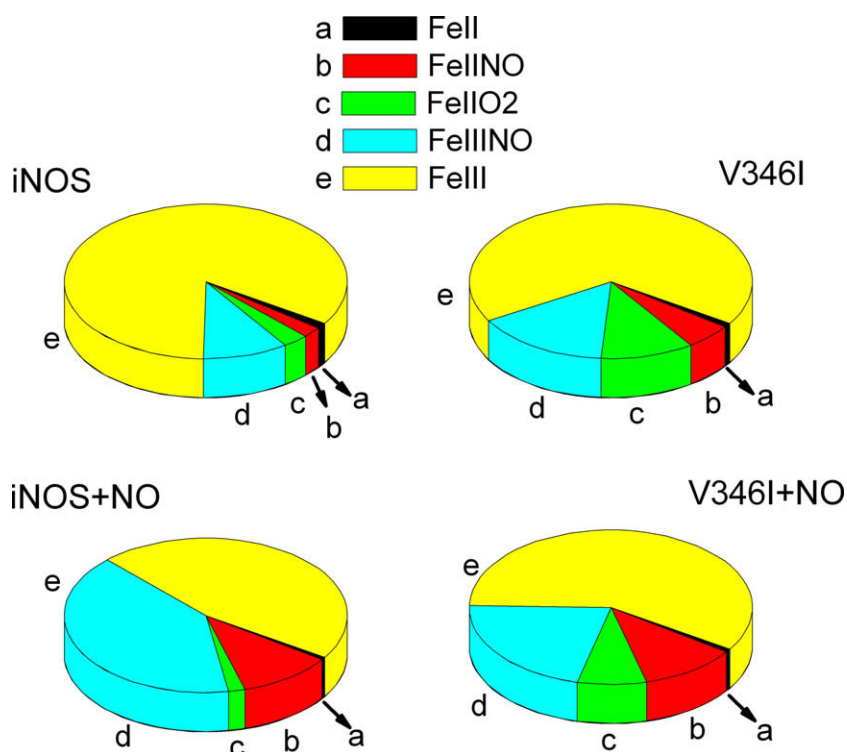


Fig. 4. NOS enzyme distribution patterns during steady-state catalytic reactions with and without 10 μ M external NO build up in solution. Computer simulations were run based on a global kinetic model (Fig. 1) as described in Section 2 assuming constant concentrations of O₂ (140 μ M) and NADPH (40 μ M).

Table 5

Simulation of steady-state catalysis and enzyme distribution in the absence and presence of 10 μM solution NO. Data are obtained by computer simulation based on global kinetic model described in Section 2 and Fig 1. WT, wild type; NA, not applicable.

	WT	V346I	WT + 10 μM NO	V346I + 10 μM NO
Fe ^{II} %	83.9	67.7	46.4	58.8
Fe ^{II} NO%	2.2	5.4	10.8	11.1
Fe ^{III} %	1.2	0.9	0.5	0.6
Fe ^{II} O ₂ %	3.0	10.7	1.9	7.9
Fe ^{III} NO%	9.7	15.4	40.4	21.6
Cit/NO	1.3	1.8	NA	NA
NO ₃ ⁻ /Cit	0.23	0.45	8.65	1.83
NO ₃ ⁻ /NO	0.30	0.81	NA	NA

performed assuming no solution NO buildup provide the minimum nitrate per citrulline (or nitrate per NO) ratios that are possible for either enzyme. These simulations indicate that V346I iNOS would generate a minimum of 0.8 nitrate per NO, much greater than the 0.3 nitrate per NO generated by wild-type iNOS. This suggests that at least 44% of the mutant enzyme cycles through the futile pathway during the steady state, as compared to 23% of wild-type iNOS.

When the simulations assume there is 10 μM NO present in solution, there is an additional pathway for nitrate formation that involves solution NO binding to the iNOS ferric heme and then being oxidized to nitrate in the futile cycle. Because this pathway consumes NADPH reducing equivalents in order to reduce the ferric heme-NO complex to ferrous (see Fig. 1), it will contribute to uncoupled NADPH oxidation. The general concept of iNOS generating and consuming its own NO has been previously proposed and discussed [19,23,27]. At 10 μM solution NO, the simulation indicates that wild-type iNOS would have a five-times greater NO dioxygenase activity than the V346I mutant (Table 5). This is because the wild-type ferric iNOS has an estimated 3-fold greater binding affinity toward solution NO (Table 2). Because NO typically builds up in solution during iNOS NO synthesis reactions in the absence of NO scavengers [19], and the solution NO can be consumed by iNOS in this manner, probably helps to explain why the wild-type iNOS generated more nitrate in its reactions (see Table 4) than the minimum amount of nitrate that was expected to form based on calculations done assuming no buildup of solution NO.

4. Conclusions

By virtue of having a fairly similar k_r and k_d and a relatively fast k_{ox} , iNOS is configured to have the greatest NO dioxygenase activity among the three mammalian NOS enzymes [23]. In the wild-type enzyme, this allows about one-quarter of the NO it generates to be destroyed in the NO dioxygenase reaction of the futile cycle, at least when O₂ concentrations are half-air saturating (about 140 μM O₂). An even greater NO dioxygenase activity is possible if the NO released by iNOS is able to accumulate in the solution. Constricting the opening to the heme pocket in iNOS via the V346I mutation alters several key kinetic parameters. This enables iNOS to form a more stable heme-superoxy intermediate, but also restricts its NO release and causes iNOS to have an almost equivalent NO release and NO dioxygenase activity. Our study highlights an important role for heme pocket geometry in balancing multiple kinetic parameters in iNOS, which in turn balance its different catalytic activities. Our results also imply that the bacterial NOS enzymes, which typically conserve the Val to Ile mutation, might in some way take advantage of the consequent kinetic changes to function in various biological settings [49].

5. Abbreviation

NOS	nitric oxide synthase
iNOS	inducible nitric oxide synthase
iNOSoxy	the oxygenase domain of inducible nitric oxide synthase
Arg	L-arginine
DTT	dithiothreitol
NO	nitric oxide
EPPS	4-(2-hydroxyethyl)-1-piperazinepropanesulfonic acid
NOHA	N ^ω -hydroxy-L-arginine
H ₄ B	(6R)-5,6,7,8-tetrahydro-L-biopterin
H ₂ B	7,8-dihydro-L-biopterin
NED	N-1-naphthylethylenediamine dihydrochloride
LDH	lactate dehydrogenase
XO	xanthine oxidase
L-NAME	NG-nitro-L-arginine methyl ester
Fe ^{II}	ferrous heme species
Fe ^{III}	ferric heme species
Fe ^{II} O ₂	ferrous oxy species
Fe ^{III} NO	ferric NO species
Fe ^{II} NO	ferrous NO species
k_r	ferric heme reduction rate
k_{ox}	ferrous heme-NO oxidation rate
k_d	ferric heme-NO dissociation rate
k_{on}	NO association to the ferric enzyme
k_{cat1}	catalytic rate constant of Arg hydroxylation
k_{cat2}	catalytic rate constant of NOHA oxidation
k_{unc}	rate of Fe ^{II} O ₂ decay to ferric enzyme and superoxide in the uncoupling reaction

Acknowledgements

This work was supported by National Institutes of Health Grants GM51491, CA53914, and HL076491 (D.J.S.), American Heart Association Beginning Grant-in-aid 0565297B (Z.-Q.W.) and KSU Summer Research and Creativity Award (Z.-Q.W.).

Appendix A. Supplementary material

Supplementary data associated with this article can be found, in the online version, at [doi:10.1016/j.jinorgbio.2009.11.006](https://doi.org/10.1016/j.jinorgbio.2009.11.006).

References

- [1] D.J. Stuehr, S. Ghosh, in: B. Mayer (Ed.), Handbook of Experimental Pharmacology, Springer-Verlag, Berlin, 2000, pp. 33–70.
- [2] W.K. Alderton, C.E. Cooper, R.G. Knowles, Biochem. J. 357 (2001) 593–615.
- [3] A.C. Gorren, B.M. List, A. Schrammel, E. Pitters, B. Hemmens, E.R. Werner, K. Schmidt, B. Mayer, Biochemistry 35 (1996) 16735–16745.
- [4] D.J. Stuehr, Annu. Rev. Pharmacol. Toxicol. 37 (1997) 339–359.
- [5] B.S. Masters, K. McMillan, E.A. Sheta, J.S. Nishimura, L.J. Roman, P. Martasek, FASEB J. 10 (1996) 552–558.
- [6] B.R. Crane, A.S. Arvai, D.K. Ghosh, C. Wu, E.D. Getzoff, D.J. Stuehr, J.A. Tainer, Science 279 (1998) 2121–2126.
- [7] T.O. Fischmann, A. Hruza, X.D. Niu, J.D. Fossetta, C.A. Lunn, E. Dolphin, A.J. Prongay, P. Reichert, D.J. Lundell, S.K. Narula, P.C. Weber, Nat. Struct. Biol. 6 (1999) 233–242.
- [8] E.A. Sheta, K. McMillan, B.S. Masters, J. Biol. Chem. 269 (1994) 15147–15153.
- [9] R. Gachhui, A. Presta, D.F. Bentley, H.M. Abu-Soud, R. McArthur, G. Brudvig, D.K. Ghosh, D.J. Stuehr, J. Biol. Chem. 271 (1996) 20594–20602.
- [10] E.D. Garcin, C.M. Bruns, S.J. Lloyd, D.J. Hosfield, M. Tiso, R. Gachhui, D.J. Stuehr, J.A. Tainer, E.D. Getzoff, J. Biol. Chem. 279 (2004) 37918–37927.
- [11] D.J. Stuehr, Biochim. Biophys. Acta 1411 (1999) 217–230.
- [12] B. Mayer, B. Hemmens, Trends Biochem. Sci. 22 (1997) 477–481.
- [13] C.-C. Wei, Z.-Q. Wang, Q. Wang, A.L. Meade, C. Hemann, R. Hille, D.J. Stuehr, J. Biol. Chem. 276 (2001) 315–319.
- [14] C.-C. Wei, Z.-Q. Wang, C. Hemann, R. Hille, D.J. Stuehr, J. Biol. Chem. 278 (2003) 46668–46673.
- [15] H. Li, T.L. Poulos, J. Inorg. Biochem. 99 (2005) 293–305.
- [16] Z.-Q. Wang, C.-C. Wei, D.J. Stuehr, J. Biol. Chem. 277 (2002) 12830–12837.
- [17] H.M. Abu-Soud, J. Wang, D.L. Rousseau, J.M. Fukuto, L.J. Ignarro, D.J. Stuehr, J. Biol. Chem. 270 (1995) 22997–23006.

- [18] S. Adak, K.S. Aulak, D.J. Stuehr, *J. Biol. Chem.* 276 (2001) 23246–23252.
- [19] H.M. Abu-Soud, K. Ichimori, H. Nakazawa, D.J. Stuehr, *Biochemistry* 40 (2001) 6876–6881.
- [20] S. Adak, Q. Wang, D.J. Stuehr, *J. Biol. Chem.* 275 (2000) 17434–17439.
- [21] A. Slama-Schwok, M. Négrerie, V. Berka, J. C. Lambry, A.L. Tsai, M.H. Vos, J.L. Martin, *J. Biol. Chem.* 277 (2002) 7581–7586.
- [22] E. Beaumont, J.C. Lambry, Z.-Q. Wang, D.J. Stuehr, J.L. Martin, A. Slama-Schwok, *Biochemistry* 46 (2007) 13533–13540.
- [23] J. Santolini, A.L. Meade, D.J. Stuehr, *J. Biol. Chem.* 276 (2001) 48887–48898.
- [24] J. Santolini, S. Adak, C.M. Curran, D.J. Stuehr, *J. Biol. Chem.* 276 (2001) 1233–1243.
- [25] S.S. Ray, J. Tejero, Z.-Q. Wang, T. Dutta, A. Bhattacharjee, M. Regulski, T. Tully, S. Ghosh, D.J. Stuehr, *Biochemistry* 46 (2007) 11857–11864.
- [26] F.H. Guo, H.R. De Raeve, T.W. Rice, D.J. Stuehr, F.B. Thunnissen, S.C. Erzurum, *Proc. Natl. Acad. Sci. USA* 92 (1995) 7809–7813.
- [27] D.J. Stuehr, J. Santolini, Z.-Q. Wang, C.-C. Wei, S. Adak, *J. Biol. Chem.* 279 (2004) 36167–36170.
- [28] J.C. Salerno, *FEBS Lett.* 582 (2008) 1395–1399.
- [29] M.M. Haque, K. Panda, J. Tejero, K.S. Aulak, M.A. Fadlalla, A.T. Mustovich, D.J. Stuehr, *Proc. Natl. Acad. Sci. USA* 104 (2007) 9254–9259.
- [30] Z.Q. Wang, C.C. Wei, S. Ghosh, A.L. Meade, C. Hemann, R. Hille, D.J. Stuehr, *Biochemistry* 40 (2001) 12819–12825.
- [31] Z.-Q. Wang, C.-C. Wei, M. Sharma, K. Pant, B.R. Crane, D.J. Stuehr, *J. Biol. Chem.* 279 (2004) 19018–19025.
- [32] S. Ghosh, D. Wolan, S. Adak, B.R. Crane, N.S. Kwon, J.A. Tainer, E.D. Getzoff, D.J. Stuehr, *J. Biol. Chem.* 274 (1999) 24100–24112.
- [33] J. Sambrook, D.W. Russell, *Molecular Cloning, A Laboratory Manual* Cold Spring Harbor Laboratory Press, 2004.
- [34] H.M. Abu-Soud, R. Gachhui, F.M. Rauschel, D.J. Stuehr, *J. Biol. Chem.* 272 (1997) 17349–17353.
- [35] D.J. Stuehr, M. Ikeda-Saito, *J. Biol. Chem.* 267 (1992) 20547–20550.
- [36] Z.-Q. Wang, C.-C. Wei, J. Santolini, K. Panda, Q. Wang, D.J. Stuehr, *Biochemistry* 44 (2005) 4676–4690.
- [37] C.-C. Wei, Z.-Q. Wang, J. Tejero, Y.P. Yang, C. Hemann, R. Hille, D.J. Stuehr, *J. Biol. Chem.* 283 (2008) 11734–11742.
- [38] M.M. Haque, M.A. Fadlalla, Z.-Q. Wang, S. Sinha Ray, K. Panda, D.J. Stuehr, *J. Biol. Chem.* 284 (2009) 19237–19247.
- [39] S. Adak, Q. Wang, D.J. Stuehr, *J. Biol. Chem.* 275 (2000) 33554–33561.
- [40] S. Adak, K.S. Aulak, D.J. Stuehr, *J. Biol. Chem.* 277 (2002) 16167–16171.
- [41] H.H.H.W. Schmidt, *Biochemica* 2 (1995) 22–23.
- [42] J. Tejero, A. Biswas, Z.-Q. Wang, R.C. Page, M.M. Haque, C. Hemann, J.L. Zweier, S. Misra, D.J. Stuehr, *J. Biol. Chem.* 283 (2008) 33498–33507.
- [43] M. Moreau, H. Takahashi, M.A. Sari, J.L. Boucher, I. Sagami, T. Shimizu, D. Mansuy, *J. Inorg. Biochem.* 98 (2004) 1200–1209.
- [44] M.A. Marletta, A.R. Hurshman, K.M. Rusche, *Curr. Opin. Chem. Biol.* 2 (1998) 656–663.
- [45] D.J. Stuehr, H.M. Abu-Soud, D.L. Rousseau, P.L. Feldman, J. Wang, *Adv. Pharmacol.* 34 (1995) 207–213.
- [46] S. Adak, M. Sharma, A.L. Meade, D.J. Stuehr, *Proc. Natl. Acad. Sci. USA* 99 (2002) 13516–13521.
- [47] S. Adak, D.J. Stuehr, *J. Inorg. Biochem.* 83 (2001) 301–308.
- [48] T. Jesús, S. Jérôme, D.J. Stuehr, *FEBS J.* 276 (2009) 4505–4514.
- [49] B.R. Crane, *Biochem. Soc. Trans.* 36 (2008) 1149–1154.